

Electronic states at polar/nonpolar interfaces grown on SrTiO₃ studied by optical second harmonic generation

A. Rubano,¹ C. Aruta,¹ U. Scotti di Uccio,¹ F. Miletto Granozio,¹ L. Marrucci,¹ T. Günter,² T. Fink,² M. Fiebig,^{2,3} and D. Paparo^{1,*}

¹CNR-SPIN and Dipartimento di Fisica, Università di Napoli “Federico II”, Compl. Univ. di Monte S. Angelo, v. Cintia, 80126 Napoli, Italy

²Helmholtz-Institut für Strahlen-und Kernphysik, Universität Bonn, Nussallee 14-16, 53115 Bonn, Germany

³Department of Materials, ETH Zurich, 8093 Zurich, Switzerland

(Received 10 October 2013; published 20 December 2013)

Optical second harmonic generation (SHG) spectra of LaAlO₃/SrTiO₃, LaGaO₃/SrTiO₃, and NdGaO₃/SrTiO₃ interfaces with SrTiO₃ substrates have been measured up to 4.2 eV as a function of film thickness and temperature. This spectral range is characterized by two-photon transitions from the valence to conduction bands of SrTiO₃ which are classified with a model based on symmetry, selection rules, and atomic orbital overlaps. This model is further confirmed in spectral measurements as a function of film thickness, material overlayer, and temperature. SHG enhancement at low temperature indicates an increase of the interfacial polarity with decreasing temperature. This confirms the relation between SHG and the spatial translation of Ti ions which are more prone to move at lower temperatures because of the quantum-paraelectric nature of SrTiO₃. We finally show that SHG spectroscopy captures structural details of the interfaces. In particular, we find evidence for proximity effects such as LaAlO₃-induced distortions of the TiO₆ octahedra or bond buckling. We also observe a correlation between SHG and the in-plane lattice mismatch between the SrTiO₃ substrate and the LaAlO₃, LaGaO₃, and NdGaO₃ overlayers.

DOI: 10.1103/PhysRevB.88.245434

PACS number(s): 73.20.-r, 73.40.-c, 77.22.Ej, 42.65.Ky

I. INTRODUCTION

As semiconductor technology is reaching its natural limit, the miniaturization to the nanoscale strongly challenges the scientific community in the search for new material classes for electronic applications. LaAlO₃/SrTiO₃ heterostructures and similar polar/nonpolar oxide interfaces are promising candidates as new materials for modern electronics and devices.¹ Since the discovery that a quasi-two-dimensional electron gas (2DEG) is formed at the interface between the two band insulators LaAlO₃ (LAO) and SrTiO₃ (STO),² an intense research effort emerged, which is unveiling a surprising array of unexpected phenomena, ranging from tunable conductivity to 2D superconductivity, including the coexistence of magnetic ordering and superconductivity.^{3–12} However, the 2DEG phenomenon is not limited to the LAO/STO interface: similar properties are reported for multiple polar-oxide heterostructures,^{13–15} for example, LaTiO₃/SrTiO₃,¹⁶ LaVO₃/SrTiO₃,¹⁷ NdGaO₃/SrTiO₃ (NGO/STO), and LaGaO₃/SrTiO₃ (LGO/STO).¹⁸ Thus, the exploitation of polar discontinuity effects has turned into a new general strategy for interfacial carrier doping¹⁹ and nanoscale device manufacturing.²⁰

The origin of the charge carriers has been a much debated question since different intrinsic and extrinsic doping mechanisms, such as cation intermixing and vacancy defects, can be at play in this oxide heterostructure.^{9,21–26} Many recent results point to the so-called *polar catastrophe scenario* as the mechanism driving the formation of the conducting state.³ According to this picture, the polar discontinuity that occurs at the interface between the charge-neutral planes of SrO and TiO₂ and the charged LaO (charge $+e$ per unit cell, where e is the electron charge absolute value) and AlO₂ (charge $-e$) sheets brings about an electrostatic breakdown

once the LaAlO₃ layer has reached a critical thickness. The polar catastrophe model has been thoroughly investigated, and the existence of a critical layer thickness for the onset of conductivity,⁴ the evolution of the conduction threshold with the formal polarization of the polar layer,²⁷ as well as the structural distortions of the LaAlO₃ layer due to an electrostriction effect^{28,29} and the effect of ion milling on the conductivity threshold³⁰ are all strong experimental evidences for the validity of this scenario.

However, many issues remain still open, such as, for instance, the prevention of the 2DEG formation when the STO substrate is terminated with a SrO plane.² In this case, not considering possible interfacial reconstructions, the SrO-terminated system is structurally identical to the TiO₂-terminated one, except for the two half-unit cells adjacent to the interface on the LAO and STO sides. However, this slight difference is sufficient to have dramatic consequences on the electronic transport properties of the interface. Examples like this one highlight the need of experimental probes suitable for investigating so-called “buried” interfaces with a nanometer and subnanometer resolution along the direction perpendicular to the interface. So far, only few spectroscopic methods have been applied to the LAO/STO interface, mainly based on electronic or photoelectronic approaches.^{31–34} They have revealed that structural transformations take place in the interfacial region before the onset of conductivity,^{35–38} but they have not resolved the controversy of whether the charge injection mechanism is dominated by the polar discontinuity or by a simpler “semiconductorlike” band-bending model.⁹ The typical probing depth of these spectroscopic techniques is 5–10 nm. Linear optical spectroscopy of the LAO/STO single interface has also been carried out,³⁹ but its interpretation is obviously hindered by the dominance of the bulk signal since both LaAlO₃ and SrTiO₃ are wide-gap transparent

crystals and their penetration depth at optical frequencies is very large. A more effective way to achieve interface-specific sensitivity approaching a single-monolayer depth is based instead on exploiting the symmetry breaking occurring at the interface.

Here, we report on optical second harmonic generation spectroscopy (SHG) of polar/nonpolar heterostructures grown on STO: LAO/STO, NGO/STO, and LGO/STO. SHG exploits the symmetry breaking at the interface and thus is an ideal tool for investigating the electronic, structural, magnetic, and dynamical properties of surfaces and interfaces with single-monolayer sensitivity.^{40–42} Within the electric dipole approximation, SHG is symmetry forbidden in the bulk of centrosymmetric materials (such as STO, LAO, NGO, and LGO), whereas interfaces and surfaces, for which the inversion symmetry is inherently broken, contribute to SHG. Thus, the SHG signal provides a probe of the polar asymmetry at the interface, with a weight given by the electron polarizability at optical frequencies. The coupling of SHG to the interfacial reorganization was unambiguously demonstrated in previous SHG experiments.^{43–47}

In Ref. 45, the presence of a surface-induced state, just below the direct STO valence-to-conduction band edge, was detected. However, the limited spectral range investigated did not allow an unambiguous assignment of this peak to a specific electronic transition from the valence-to-conduction band. Associating each spectral feature to a specific electronic transition is essential for all future applications of SHG spectroscopy to STO-based oxide heterostructures. Recently, a model based on symmetry-controlled selection rules and orbital overlap made this possible.⁴⁷ However, in Ref. 47 the investigation was limited to LAO/STO samples with a fixed thickness of the LAO film, measured at room temperature. Here, we vary different parameters: the thickness of the overlayer film, the temperature, and the chemistry of the deposited film. This allows a detailed check of the symmetry-controlled selection rules at play in the SHG spectroscopy of these interfaces. As a general observation, we find that the aforementioned symmetry-controlled selection rules are universally valid for these material systems as far as the interfacial cubic symmetry is preserved. The experimental confirmation of this model provides a useful framework for further SHG investigation of analogous polar/nonpolar interfaces. On the one hand, we have found an overall enhancement of SHG signal at low temperature, indicating an increase of the interfacial polarity. This confirms the picture about the origin of SHG as a consequence of the spatial translation of Ti ions. The latter are more prone to move at low temperature, when STO comes to the verge of a ferroelectric state.^{43,45,47} On the other hand, there are some exceptions where we observe noticeable deviations from the general behavior imposed by symmetry selection rules. This demonstrates that this symmetry is partly lifted due to proximity effects, as, for example, distortions of the TiO₆ octahedra possibly induced by LAO in STO at the interface or bond buckling. Finally, we observe an interesting correlation between the SHG signal and the in-plane lattice mismatch of LAO/STO, NGO/STO, and LGO/STO interfaces. All these findings show the potential of the SHG spectroscopy in capturing subtle structural details of these interfaces.

II. GENERAL THEORY OF SURFACE SECOND HARMONIC GENERATION

Here, we recall the main points of a theory that has been published elsewhere.⁴⁸ SHG is the nonlinear process giving rise to a light wave with doubled frequency 2ω from an incident wave of frequency ω . The constitutive equation of the process, representing the material response, is

$$P_i(2\omega) = \varepsilon_0 \chi_{ijk}(2\omega) E_j(\omega) E_k(\omega), \quad (1)$$

where $\mathbf{P}(2\omega)$ is the induced nonlinear optical polarization, $\mathbf{E}(\omega)$ is the local (complex) electric field of the incident wave at the interface, and the tensor $\hat{\chi}$ is the SHG susceptibility. We assume here and in the following that the tensor $\hat{\chi}$ is nonzero only within a thin interfacial (polar) region in which the inversion symmetry is removed, while the bulk of both the substrate (the STO) and the deposited thin film (the LAO, LGO, and NGO) are centrosymmetric and hence have a vanishing $\hat{\chi}$. Moreover, we neglect the possible contribution to SHG from the free LAO, LGO, or NGO surface, although it also breaks the inversion symmetry. To support these assumptions, we have performed SHG experiments on bare LAO, LGO, and NGO substrates, finding a signal that is always well below the level measured in bare STO.⁴⁵ This is a consequence of the large direct band gap of these materials as compared to SrTiO₃.

The electronic properties of the polar interface are reflected in the spectral dependence of the nonzero tensor components of $\hat{\chi}$. The actual measured quantity in SHG spectroscopy is the SHG intensity I_{SHG} as a function of the incident photon energy ω , which is proportional to the square of the reflected SHG electric field: $I_{\text{SHG}} \propto |E_{\text{SHG}}|^2$. Exploiting Eq. (1) and the theory of light propagation through stratified media, the latter can, in turn, be written as a function of the incident electric field:

$$E_{\text{SHG}} = \frac{i\omega E_0^2}{\varepsilon_0 c \cos \beta} \chi^{\text{eff}}, \quad (2)$$

where c is the speed of light in vacuum, ε_0 is the dielectric constant in vacuum, E_0 is the electric field amplitude of the impinging wave, β is the incidence angle respect to the surface normal, and χ^{eff} is defined as follows:

$$\chi^{\text{eff}} = \int e_i^{\text{out}} L_{ii}^{\text{out}} \chi_{ijk} L_{jj}^{\text{in}} L_{kk}^{\text{in}} e_j^{\text{in}} e_k^{\text{in}} dz, \quad (3)$$

$\mathbf{e}^{\text{in, out}}$ being the optical polarization unit vectors in vacuum (or in air, if the small refractive index difference is neglected) of the input and output waves, respectively, and $\mathbf{L}^{\text{in, out}}$ are the corresponding Fresnel transformation matrices accounting for the propagation from/to the outside of the medium to/from the interfacial polar layer, whose explicit expression may be found in Ref. 48. Here, the sum over repeated indices is implied and the z integral is extended across the entire thickness of the polar interface, which is assumed to be much thinner than the optical wavelength λ . In other words, χ^{eff} defines a suitable combination of $\hat{\chi}$ tensor components inside the material defined by the input/output light polarizations and accounting for all transmission/reflection effects through the boundaries.

A. Optical transitions at the Γ point of STO-based heterostructures

In the investigated range of SHG photon energy, it has been established that the SHG source resides in the STO side of the interface.⁴⁵ This is a consequence of the width of the STO band gap as compared to LAO, LGO, and NGO, whose resonant contribution may be found at higher energies. Therefore, we focus our attention on the bulk STO structure and symmetries, and discuss the expected changes due to the interface-induced symmetry breaking. Moreover, since the investigated range is close to the interband transition edge, we will limit our analysis to the symmetry valid at the Γ point of the Brillouin zone (BZ). The bulk STO optical gap is known to be associated mainly with a transition from the oxygen $2p$ orbitals to the titanium $3d-t_{2g}$ ones. The STO electronic band structure has been calculated, for example, in Refs. 49–51.

At the Γ point of the bulk Brillouin zone, the oxygen bands may be grouped in three levels depending on the relative arrangement of the $2p$ orbitals, as schematically shown in Fig. 1(a): bonding, nonbonding, and antibonding. Each of these levels is threefold degenerate in the bulk, owing to the cubic symmetry of the crystal. The minimum optical (vertical) transition energy, at the Γ point, is known to be 3.75 eV. The

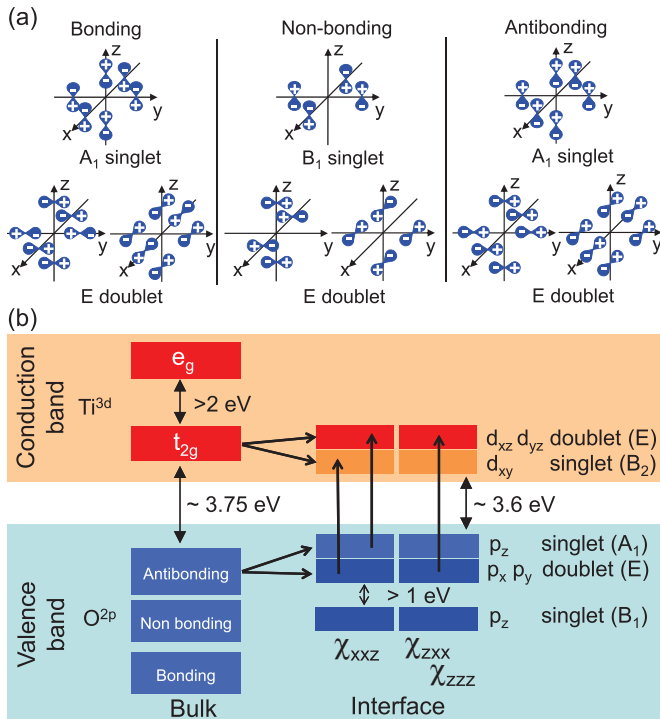


FIG. 1. (Color online) In panel (a), the possible arrangements of O ($2p$) orbitals forming the nine upmost valence bands are indicated. In the bulk, they are grouped in triply degenerate levels according to the cubic $m3m$ symmetry. At the surface, this degeneracy is partly lifted by the local $4mm$ symmetry with the separation among singlet and doublet states as indicated. Panel (b) shows the symmetry-allowed O($2p$)-Ti($3d$) 2ω transitions for all three symmetry-allowed χ_{ijk} components within the $4mm$ symmetry group. According to Eq. (5), the allowed transitions for χ_{zzz} (contributing to the pp signal together with the other χ elements) and χ_{zxx} (sp signal) are the same, whereas two different transitions are allowed for χ_{xxz} (ds signal).

one at the X point is only slightly higher, by about 1 eV, and has a similarly high density of states. Therefore, it might contribute with additional visible features in the SHG spectra.

The conduction band is predominantly composed of Ti $3d-t_{2g}$ orbitals. Because of the cubic crystal field produced by the six nearest-neighbor O atoms, the empty Ti $3d$ orbitals will split into three lower-energy t_{2g} orbitals (xy, yz, zx) and two higher-energy e_g orbitals ($3z^2 - r^2, x^2 - y^2$).⁵² The t_{2g} - e_g splitting of the Ti $3d$ orbitals is of about 2 eV. The Sr $4d$ bands have their peak density of states about 5 eV above the Ti bands. The symmetry lowering from a cubic 3D symmetry to the square 2D one ($4mm$) further splits the Γ point bands. In particular, the three Ti $3d-t_{2g}$ orbitals (corresponding to d_{xy}, d_{xz}, d_{yz}) split into two different levels: the orbital d_{xy} with symmetry B_2 and the two degenerate orbitals d_{xz} and d_{yz} forming an E doublet. The two Ti $3d-e_g$ orbitals, in turn, split into A_1 and B_1 singlets, namely, d_{z^2} and $d_{x^2-y^2}$. On the other hand, the three oxygen levels are split into six distinct levels: three singlets and three doublets. Considering the center of the cubic cell to be placed on the Ti ion, the orbitals of the oxygens lying along the z direction (vertical axis of the octahedron) give rise to an A_1 singlet band (p_z) and an E doublet band (p_x, p_y), while the orbitals of the oxygens lying in the TiO_2 plan can be combined into an A_1 band, made of parallel p_z orbitals, a B_1 band, made of antiparallel p_z orbitals, and two different E doublets formed by the p_x and p_y orbitals [see Fig. 1(a)].

B. Surface SHG selection rules

Since the crystal structure of our materials is perovskitelike, our polar/nonpolar interfaces have a fourfold rotation symmetry and mirror planes that are perpendicular to the surface and contain the two in-plane principal symmetry axes. Therefore, they belong to the $4mm$ Laue group (in Hermann-Mauguin notation, or C_{4v} in Schoenflies notation). Within the $4mm$ symmetry, it can be shown that only the following three independent nonvanishing tensor components are allowed for the the $\hat{\chi}$ tensor:⁵³

$$\begin{aligned} \chi_{zzz}, \\ \chi_{zxx} = \chi_{zyy}, \\ \chi_{xxz} = \chi_{yyz} = \chi_{xzx} = \chi_{yzy}. \end{aligned}$$

The last two components can be singled out in χ^{eff} by an appropriate choice of the input and output polarizations, while the diagonal component χ_{zzz} is always present in combination with the other two. Here, we indicate with p , d , and s a linear polarization that is, respectively, parallel, perpendicular, and at 45° with respect to the incidence plane. In particular, we report the expression of χ^{eff} for the s -input p -output (sp) and the d -input s -output (ds) polarization combinations, which contain χ_{zxx} and χ_{xxz} , respectively, and for the p -input p -output (pp) combination, which contains all three components:

$$\begin{aligned} \chi_{sp}^{\text{eff}} &= \chi_{zxx} t L_{zz}^{\text{out}} (L_{yy}^{\text{in}})^2 \sin \beta, \\ \chi_{ds}^{\text{eff}} &= \chi_{xxz} t L_{yy}^{\text{out}} L_{yy}^{\text{in}} L_{zz}^{\text{in}} \sin \beta, \\ \chi_{pp}^{\text{eff}} &= \chi_{zzz} t L_{zz}^{\text{out}} (L_{zz}^{\text{in}})^2 \sin^3 \beta + (\chi_{zxx} t L_{zz}^{\text{out}} L_{xx}^{\text{in}} \\ &\quad - 2\chi_{xxz} t L_{xx}^{\text{out}} L_{zz}^{\text{in}}) L_{xx}^{\text{in}} \sin \beta \cos^2 \beta, \end{aligned} \quad (4)$$

where t denotes the effective thickness of the polar interface. The χ_{ijk} components in this expression are actually space-averaged quantities across this thickness. We note that, unlike the standard optical techniques, the probing depth of SHG is not *a priori* fixed, but depends on the spatial extension of the polar asymmetry at the specific interface under study.

Using the approximate value of 2.3 for the STO refractive index at the fundamental wavelength (around 800 nm) and of 2.4 at the SHG wavelength (around 400 nm), one can calculate that the coefficient in front of the χ_{zzz} component in the χ_{pp}^{eff} expression is about a factor 20 smaller than the coefficients in front of χ_{xxz} and χ_{xxz} for $\beta = 45^\circ$; for $\beta = 80^\circ$ (about grazing incidence), this ratio is still about 10. This implies that it is not possible to isolate experimentally the χ_{zzz} contribution, which can only be estimated *a posteriori* once χ_{xxz} and χ_{zxx} are determined, by a delicate subtraction procedure. This has been done, for example, in Ref. 45, but it is not needed for the following analysis.

At the Γ point and for 2ω transitions between a valence state V and a conduction state C a simple symmetry argument can be used for obtaining the relevant optical selection rules (more details may be found in Ref. 48). For a 2ω resonance, these rules are dictated only by the spatial parity of the $\hat{\chi}$ output index coordinate, which is associated with the emission of the second harmonic photon. The $\hat{\chi}$ index variables z and x correspond to the $4mm$ group representations A_1 and E , respectively. We can use then the table of the representation products for the $4mm$ group, as given, for example, in Appendix B of Ref. 54, to obtain the following selection rules:

$$\begin{aligned} \chi_{zzz} \neq 0, \chi_{zxx} \neq 0, \chi_{xxz} = 0, \\ \text{if V, C have the same symmetry} \\ \chi_{zzz} = 0, \chi_{zxx} = 0, \chi_{xxz} \neq 0, \\ \text{if V, C have different symmetry, one being } E \quad (5) \\ \chi_{zzz} = 0, \chi_{zxx} = 0, \chi_{xxz} = 0, \\ \text{if V, C have different symmetry, none being } E. \end{aligned}$$

By exploiting these rules, each single $\hat{\chi}$ element may be linked to a specific atomic orbital character of the electronic bands at the polar/nonpolar interface, as it has been done in Ref. 48. The results of the latter analysis are summarized in Fig. 1(b). In particular, we find that χ_{zxx} (sp) and χ_{zzz} are characterized by the $O(p_x, p_y) \rightarrow \text{Ti}(d_{xz}, d_{yz})$ transition, while in χ_{xxz} (ds) both $O(p_x, p_y) \rightarrow \text{Ti}(d_{xy})$ and $O(p_z) \rightarrow \text{Ti}(d_{xz}, d_{yz})$ transitions are present.

Being solely based on symmetry considerations, the scheme reported in Fig. 1(b) is valid for both insulating and conductive interfaces. However, a quantitative difference in the energetic positions of the electronic transitions may be expected for interfaces with different conductance and overlayer chemistry. This information can not be obtained only through our symmetry analysis. Angle-resolved photoemission spectroscopy data on STO surfaces,⁵⁵ x-ray absorption spectroscopy on LAO/STO,^{35,38} and theoretical calculations^{56,57} show that the lowest conduction band is given by d_{xy} orbitals, but this is not enough to assign an energetic hierarchy to our SHG electronic transitions because optical transitions are obviously affected by the valence bands too. We need additional information

such as those provided by our SHG results discussed in the following and in our past works.⁴⁷ Finally, we stress that this simplified picture is only valid close to the Γ point, while elsewhere in the Brillouin zone the symmetry is broken by the crystal momentum \mathbf{k} .

III. EXPERIMENT

A. Film preparation

Films of LaAlO_3 , NdGaO_3 , and LaGaO_3 were prepared by pulsed laser deposition on STO(001) substrates having TiO_2 termination while controlling the film thickness on a unit-cell scale by means of high-energy electron diffraction (RHEED) oscillations. The samples were grown at $\approx 800^\circ\text{C}$ in 1×10^{-4} mbar oxygen atmosphere and then cooled at the same pressure to room temperature. For LAO/STO samples, we have varied the number n of unit cells (u.c.) over a wide range: $n = 1, 2, 3, 4, 6, 9, 10, 12$. Interfacial conduction (sheet conductance $\sigma_S = 10^{-5} - 10^{-4} \Omega^{-1}$ at 300 K) emerges at four monolayers of LAO coverage, while all the $n < 4$ samples show a sheet conductance below the detection limit of $10^{-9} \Omega^{-1}$. In the case of LGO/STO and NGO/STO interfaces, we have selected two representative thicknesses, $n = 2$ and 12, that give samples below and above the conductive threshold, respectively. Both conductive NGO/STO and LGO/STO samples have a sheet conductance comparable with that of conductive LAO/STO interfaces.

B. SHG spectroscopy

The SHG signal is induced by means of wavelength-tunable laser pulses. An amplified Ti:sapphire laser generates 130-fs pulses having a central wavelength of 800 nm and a repetition rate of 1 kHz. The pulses are sent to a collinear optical parametric amplifier, which can tune the central wavelength of the pulse within a large infrared-to-visible spectral range. The pulse is then focused onto the sample surface with an incidence angle of 45° , and typical input fluence of about 3–5 mJ/cm². The emerging SHG signal is measured in a reflection geometry. A filter cuts off the fundamental frequency and a monochromator is used to further increase the spectral rejection. The signal is then measured by means of a broad-band photon multiplier and sent to the data acquisition system. In order to account for the spectral response function of the experimental setup, the as-recorded spectrum has been normalized to the SHG signal from an aluminum surface, which presents a flat and featureless SHG spectrum in the whole investigated spectral range. All the measurements presented here have been performed in air at room temperature, except for a subset of LAO/STO interfaces that have been investigated in the interval from 10 to 300 K.

IV. EXPERIMENTAL RESULTS

A. SHG spectra of LAO/STO interfaces as a function of LAO thickness

Figure 2 shows the pp , ds , and sp spectra for LAO coverage n ranging from 0 to 12 monolayers in the two-photon energy range between 3.2 and 4.2 eV. In the range between 1.5 and

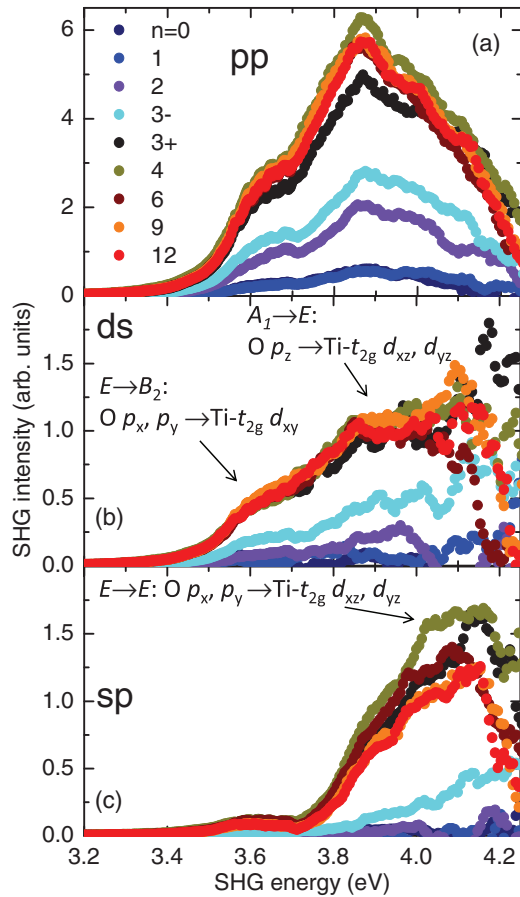


FIG. 2. (Color online) SHG spectra obtained from LAO/STO heterostructures up to 4.2 eV for (a) *pp*, (b) *ds*, and (c) *sp* polarization configurations for different LAO thickness. Note that samples with $n = 3$ exhibit a strong sample-to-sample spread of the SHG yield. This value of n matches the threshold value for a discontinuous structural transition preceding the onset of conduction, as explained in the text. Thus, we show the extreme cases, naming “3+” the sample whose SHG signal is approximately as high as samples with $n > 3$, and “3-” the sample with SHG signal comparable to samples with $n < 3$. The spectral range covers the direct $O(2p) \rightarrow Ti(3d)$ cross-gap transition of STO, which shows up as an increase of the SHG intensity at around 3.6 eV. Symmetry-based SHG selection rules explain the fact that the lowest-energy transition at 3.6 eV is present as a shoulder in the spectrum of *pp* and *ds*, whereas it is mostly absent in *sp* polarization configuration. Note that the same reference scale (in arbitrary units) is used in all three panels.

3.2 eV, all spectra are flat and featureless, while the range above 4.2 eV is difficult to access for the lack of suitable polarization optics. The first observation deduced from the SHG spectra is an increase of the SHG intensity in all samples at around 3.6 eV, which nicely matches the edge of the direct $O(2p) \rightarrow Ti(3d)$ cross-band-gap transitions in STO. This was already observed in a previous work by some of us.⁴⁵ However, given the limitation of the investigated spectral range, it was not evident that the slope of the *pp* spectra up to 3.7 eV was part of a major peak at around 3.8 eV. This peak is in good agreement with the peak of the dielectric function revealed by ellipsometry data found in literature.^{58,59} This finding further confirms the presence of the optical valence-to-conduction

band edge in the SHG spectra. From this evidence, it can be safely stated that SHG probes the electronic composition of the STO layers adjacent to the interface and thus the structure of the $O(2p)$ and $Ti(3d)$ orbitals involved.

The second information element is obtained by comparison of the SHG spectra for a varying thickness of the LAO overlayer, as expressed in terms of the number n of unit cells. The overall SHG yield is small for $n = 0, 1$ and starts to increase for $n = 2$. For $n = 3$, an abrupt and substantial increase of the SHG intensity in all components and over the entire spectral range takes place. Note that samples with $n = 3$ exhibit a strong sample-to-sample spread of the SHG yield. This value of n matches the threshold value for a discontinuous structural transition preceding the onset of conduction reported in former SHG experiments.^{43,45} Thus, we show the extreme cases, naming “3+” the sample whose SHG signal is approximately as high as samples with $n > 3$, and “3-” the sample with SHG signal comparable to samples with $n < 3$. It is important to stress here that, notwithstanding the variation of the SHG signal, all the $n = 3$ samples remain insulating. The detailed origin of the sample-to-sample variations at $n = 3$ is unknown. However, it is plausible that samples close to the reconstruction threshold are particularly sensitive to tiny changes in growth conditions or to atmospheric adsorbates once exposed to air after deposition. However, after this possible initial modification, the sample properties remain eventually stable in air. In fact, the qualitative behavior of the $n = 3$ samples remained unchanged since the very first SHG measurements.⁴³ Samples with $n > 3$ show only a slight further increase of the SHG yield with respect to the $n = 3+$ sample. Hence, the saturation of the SHG intensity at $n = 3$ indicates that the interface is electronically fully reconstructed. In particular, no major changes of SHG, such as a step-like increase, are observed between $n = 3+$ and $n = 4$, i.e., at the threshold for the formation of the 2DEG.

B. SHG spectra of LAO/STO interfaces as a function of temperature

SHG spectroscopy experiments have been performed on five LAO/STO samples at varying temperature down to 10 K. SHG spectra ranging from 3.2 to 4.2 eV were recorded at 10, 80, 120, and 300 K. In particular, 80 and 120 K are, respectively, below and above the temperature where STO displays a second-order phase transition from the cubic ($Pm\bar{3}m$) to an antiferrodistortive tetragonal ($I4/mcm$) phase. This phase transition is reported to occur at 105 K.⁶⁰ With respect to the analysis of symmetries discussed in the following, it is important to emphasize that both these space groups have a fourfold symmetry in the interface plane.

In Fig. 3, the SHG spectra for all three polarization combinations from a pure STO substrate (left column) and a representative conducting LAO/STO interface with $n = 10$ layers of LAO (right column) are shown. The spectra were normalized using the procedure described above and, in addition, accounting for the change of the refractive index in STO at low temperature.⁵⁹ No abrupt qualitative and quantitative change of the SHG spectra between 120 and 80 K was observed. Thus, all physical properties probed by SHG

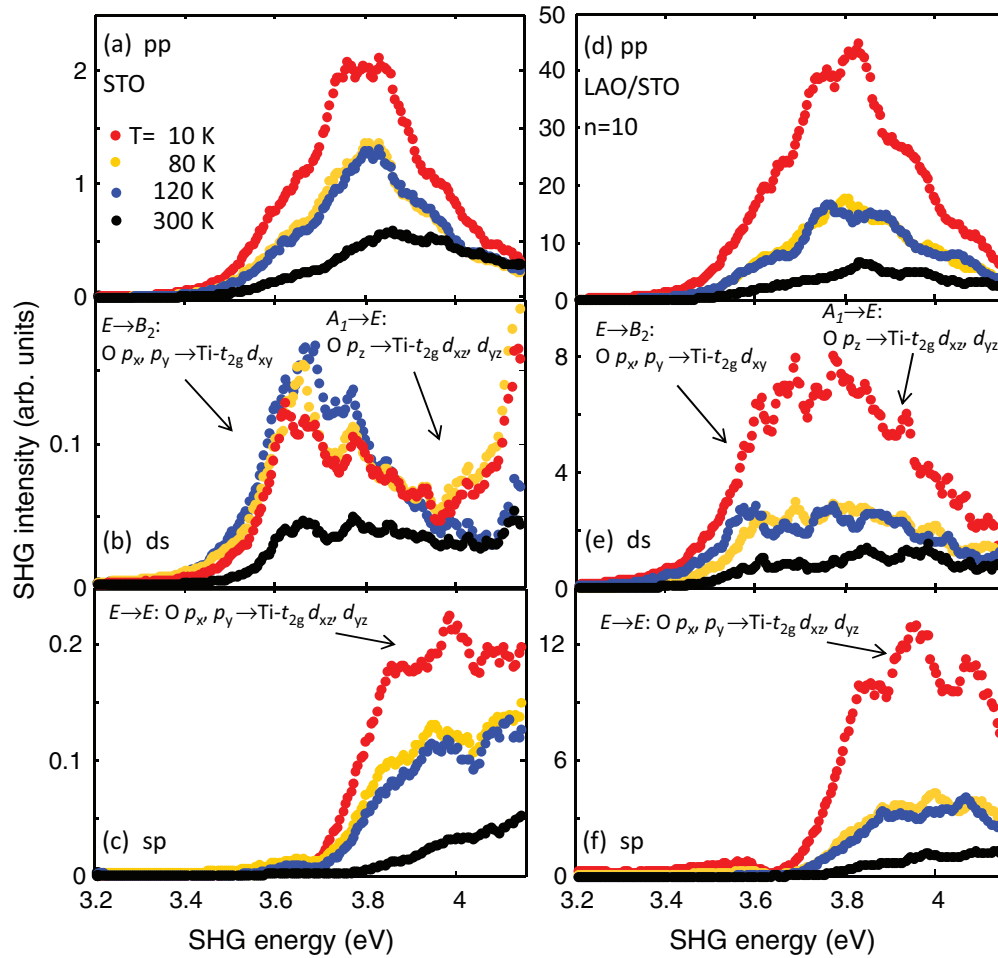


FIG. 3. (Color online) Comparison of the SHG spectra of a pure STO substrate ($n = 0$, left column) and a conducting LAO/STO interface ($n = 10$, right column) at 300 and 10 K for pp (a), (d), ds (b), (e), and sp (c), (f) polarization combinations. Note that the same reference scale (in arbitrary units) is used in all six panels.

are reflected in the spectra taken at 300 and 10 K. Moreover, all qualitative changes between conducting and nonconducting samples are captured by the set of spectra shown in Fig. 3.

Once again, one finds that the qualitative shape of all the polarization combinations in the pure STO sample is reproduced in the $n = 10$ samples, as formerly reported for the room-temperature spectra of Fig. 3. This finding confirms the previous conclusion that the main source of the SHG signal is located within the STO interfacial layers. Note that significant quantitative differences are apparent at the lowest temperature as compared to the room-temperature spectra. Aside from an enhanced SHG intensity, which is observed in all components and all samples with decreasing temperature, it is interesting to note that the peak around 3.8 eV in the pp and ds spectra is enhanced more than the other spectral components for both STO and LAO/STO samples. Finally, at the lowest temperature, it is evident that the total number of resonances revealed by the SHG spectra exceeds the number of those identified by the SHG selection rules. In particular, we observe additional peaks around 3.7 and 3.8 eV in pp and ds spectra, and around 3.9 eV in sp spectra. Both these results will be discussed further in Sec. V.

C. SHG spectra of polar/nonpolar interfaces as a function of the overlayer material

In Fig. 4, a comparison between the SHG spectra of LAO/STO, LGO/STO, and NGO/STO interfaces is shown. It is evident that all samples share the same qualitative behavior. Once again, this confirms that SHG is probing the electronic interband transitions of STO. However, we can also highlight a few quantitative differences with respect to the specific overlayer. In particular, within the same class of samples (insulating or conductive), the SHG signal of the LAO/STO samples is always larger than that of the other two interfaces. This might be a consequence of the observed greater sharpness of LAO/STO interfaces as compared to LGO/STO and NGO/STO interfaces.¹⁸ Moreover, for the ds and pp spectra of the 12 u.c. samples, we find that the high-energy part of the spectra (approximately the 3.8–4.0 eV interval), is less enhanced in LGO/STO and NGO/STO samples than in LAO/STO, when compared to the 3.6-eV peak. Finally, if we focus our attention on the pp spectra of the 2 u.c. samples [triangles in Fig. 4(a)], we see that the overall SHG signal for the LAO/STO interface is bigger than for the NGO/STO and LGO/STO samples, with the latter giving the lowest signal. We will discuss this observation in detail in the following.

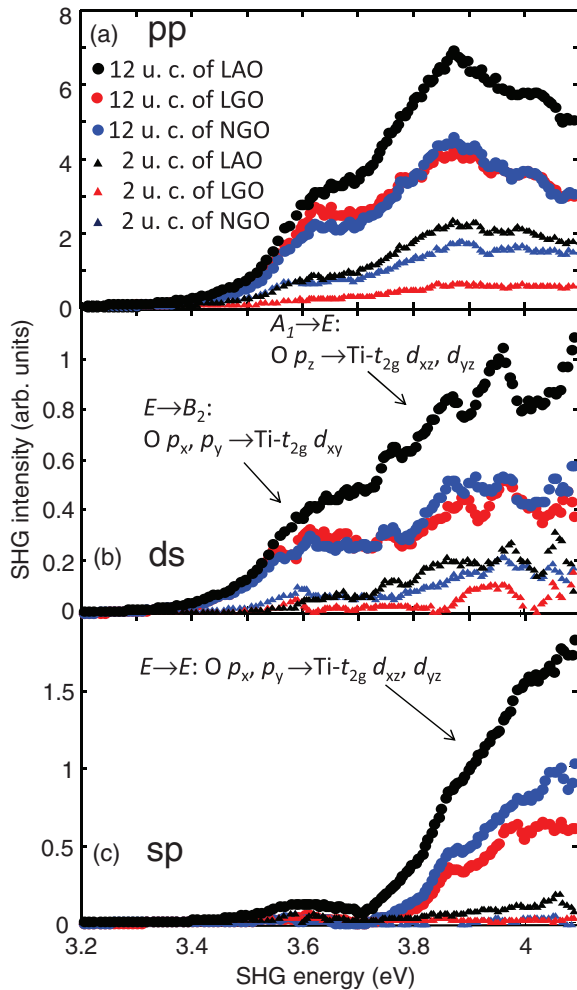


FIG. 4. (Color online) Comparison between the SHG spectra of LAO/STO (black symbols), LGO/STO (red symbols), and NGO/STO (blue symbols). For each material, we compare two thicknesses of the overlayer: 2 (circles) and 12 (triangles) unit cells. The interfaces with an overlayer of 2 unit cells are insulating, while those with 12 unit cells are conductive. Note that the same reference scale (in arbitrary units) is used in all three panels.

V. DISCUSSION

We recall that, under dipole approximation, the SHG signal reflects the polarity (polar asymmetry) of the orbitals, arising from the changes occurring in their environment. The atomic orbital polarity is caused by the proximity to the interface, while in the bulk it must vanish by symmetry. A small nonlocal contribution generated inside the bulk of STO and not related to the interfacial breaking of the inversion symmetry could also be present,⁶¹ but it is independent on the thickness and material of the ultrathin film overlayer. Therefore, all the qualitative results of the comparison between our samples can not be affected by this possible spurious signal.

The threshold behavior observed in the SHG spectra as a function of the LAO thickness and its origin has been already discussed in our previous work.⁴⁵ However, here, thanks to the extended spectral interval and range of physical parameters investigated, we consolidate and refine our earlier interpretation. Briefly, SHG indirectly senses the charge asymmetry

at the interface. When a space-charge region is created at the interface, this develops an electric field that polarizes all the orbitals involved in the SHG spectra (for example, by displacing the Ti ions). Therefore, when charge injection occurs at the onset of conduction, the SHG signal is enhanced. We find, however, that the SHG signal is already large at $n = 3$, and to a lesser extent at $n = 2$, meaning that SHG is actually probing a “precursor” of the onset of conduction: charges start to be injected, but they are localized, so that they contribute to the interfacial field buildup. We note that if the injected charges, both trapped or mobile, accumulated exactly at the interface, within the first atomic layer, they would provide a perfect screening of the LAO polarization with no electric-field buildup in the STO. Instead, the injected charges spread over few unit cells of STO, mainly because of electronic kinetic energy, thus creating an inhomogeneous distribution of charges and, consequently, an electrostatic field that spatially decays in STO.¹⁸

It is remarkable that in terms of the SHG data the emergence of conduction is clearly separated from the orbital reconstruction. A variety of mechanisms may contribute to this: (i) SHG may be less sensitive to mobile than to localized carriers; (ii) application of the fourth LAO monolayer may free some of the carriers trapped at $n = 3$, so that the total number of carriers at the interface (and the associated SHG yield) may not change; (iii) the number of carriers contributing to conduction may be much smaller than the number of trapped carriers contributing to the orbital reconstruction.

This picture applies to LGO/STO and NGO/STO interfaces, too. Indeed, they show an analogous behavior with the enhancement of the SHG signal between 2 and 12 unit cells. This result is not linked to the specific shape of the SHG spectra. By including the latter, we can now add more details to our understanding of the spectra obtained on STO-based heterostructures. According to Fig. 1(b), the χ_{zxx} (sp) and χ_{xxz} (ds) spectra should look rather different since they probe distinctly different electronic transitions. This is indeed evident by an inspection of Figs. 2(b) and 2(c). In particular, in Fig. 2(b), we note the presence of a peak at about 3.6 eV, that is almost absent in the sp spectrum. In Ref. 47, the peak at 3.6 eV has been assigned unambiguously to the transition $E \rightarrow B_2: O p_x, p_y \rightarrow Ti-t_{2g} d_{xy}$. The latter is allowed in χ_{xxz} and forbidden in χ_{zxx} , thus explaining the large suppression of this peak in the sp spectrum, as compared to the high-energy part of the spectrum. Drawing such a definite conclusion was not possible in Ref. 45 because of the more limited investigated spectral range of that work which did not include the main peaks located at 3.8–4.1 eV. Here, instead, the action of the above-described selection rules becomes fully evident.

According to the general symmetry arguments described in Sec. II, the latter result must be valid as long as the interface $4mm$ symmetry is not varied. Therefore, if this symmetry is unperturbed by varying temperature, overlayer thickness, or material, we must continue to observe a substantial suppression of the peak at 3.6 eV in all the sp spectra. This is indeed the case, as found by an inspection of Figs. 2(b) and 2(c), 3(b) and 3(c), 3(e) and 3(f), and 4(b) and 4(c). This agrees with the fact that none of these parameters changes the $4mm$ symmetry of the interface.

Actually, although being strongly attenuated, the peak at 3.6 eV is not entirely suppressed in all the *sp* spectra [see, for example, Figs. 2(c), 3(c), 3(f), or 4(c)]. This might mean that the $4mm$ symmetry is, at least weakly, broken at the interface. This can result, for example, from the oxygen octahedron rotations and the TiO_6 octahedra distortions possibly induced by LAO in STO at the interface.⁶² Bulk STO is characterized by a cubic lattice without significant rotation of the oxygen octahedra, while bulk LAO is rhombohedral with significant octahedra rotation. At the interface, the two oxygen sublattices are coupled, and the discontinuity in the rotation angle may induce a structural reconstruction involving octahedral deformations. The latter effect might partly lift the $4mm$ symmetry leading to the appearance of a small SHG contribution at 3.6 eV in the *sp* spectra.

As already noted, the spectra recorded at different temperatures confirm the general picture based on the selection rules described above. However, a closer look at the spectra highlights several additional and interesting spectral features. First, we note that the overall SHG signal displays a huge increase when temperature decreases. This is very likely connected to the quantum paraelectric behavior of STO at low temperatures. It is well known that at low temperatures the Ti ions are more prone to be displaced. We expect that this tendency may enhance the polarization asymmetry of the interface and probably also extends the penetration length of the polar region, thus leading to an amplification of the SHG signal for decreasing temperature. Second, if we focus our attention on the spectra recorded at 10 K, it is evident that the central resonance around 3.8 eV, for the *pp* and *ds* polarization combinations, is enhanced more than the highest-energy part of the spectrum. In contrast, for the *sp* polarization combination, the enhancement appears to be uniform across the spectrum. By recalling again the results of Ref. 47, we find that the central SHG resonances were assigned to the transition $A_1 \rightarrow E: O p_z (A_1) \rightarrow \text{Ti-}t_{2g} d_{xz}, d_{yz}$, in the case of the *ds* polarization combination, and to the transition $E \rightarrow E: O p_x, p_y \rightarrow \text{Ti-}t_{2g} d_{xz}, d_{yz}$, in the case of *sp* (while the *pp* case includes both contributions). These two transitions differ only for the initial valence state: p_x, p_y for *sp* and p_z for *ds*, respectively. Therefore, the observed stronger enhancement of the central resonance in the *pp* and *ds* spectra may be attributed to a larger increase of the orbital polarizability of p_x, p_y orbitals than for p_z orbitals, possibly due to in-plane bond distortions.

Finally, at the lowest temperature, the presence of additional peaks becomes more distinct. This might be linked to the presence of different subbands, as observed at low temperature also by angle resolved photoemission spectroscopy (ARPES).⁵⁵ It is likely that at low temperature the degeneracy of the d_{xz}, d_{yz} bands, as well as that of the p_x, p_y bands, is at least partially lifted. On one hand, the energy splitting of the resonances around 3.6 and 3.8 eV of about 90 meV is reminiscent of the d_{xz}, d_{yz} orbital splitting of about 60 meV, as measured by ARPES in STO. On the other hand, the peak splitting in *sp* around 3.9 eV of about 120 meV is in good agreement with the separation of the two d_{xz}, d_{yz} subbands, possibly resulting from electron-confinement effect, spin-orbit coupling, and/or low-temperature tetragonal/orthorhombic distortions, as again indicated also by ARPES (see Ref. 55 for

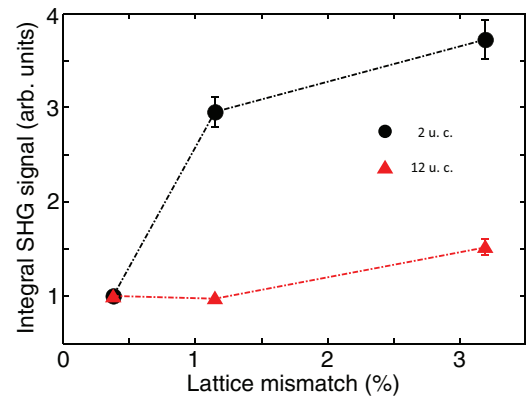


FIG. 5. (Color online) Spectrally integrated SHG signal of the *pp* polarization combination as a function of the substrate/overlayer in-plane lattice mismatch for 2 u.c. (circle) and 12 u.c. (triangle) samples, respectively. As explained in the text, per each data set, the reported SHG signal is obtained by integrating the *pp* spectra over the 3.2–4.1 eV energy range and normalizing it to the corresponding sample with the lowest lattice mismatch. Lines are guides to the eye.

a more detailed description). Another possible explanation for this behavior might be related to enhanced oxygen octahedra rotations at the interface. Hence, in absence of more detailed *ab initio* calculations, a clear assignment of these energy features remain speculative. Therefore, we indicated in the figures only the electronic transitions reported in the scheme of Fig. 1(b) that are obtained from generally valid symmetry arguments.

Finally, we briefly discuss the SHG spectra of the two-unit cells LAO/STO, LGO/STO, and NGO/STO samples. As already noted, the *pp* signal of the LAO/STO interface is bigger than NGO/STO and LGO/STO interfaces, with the latter giving the lowest signal. Interestingly, the SHG signal hierarchy observed in these samples follows that of the lattice mismatch between the deposited material and the substrate, being 0.38%, 1.15%, and 3.20% for LGO/STO, NGO/STO, and LAO/STO, respectively.⁶³ This is shown in Fig. 5, where we plot the integrated SHG signal for the *pp* spectra as a function of the lattice mismatch. Per each data set, the reported SHG signal is obtained by integrating the *pp* spectra over the 3.2–4.1 eV energy range and normalizing it to the corresponding sample with the lowest lattice mismatch. In the case of the 2 u.c. samples we note an increase of this signal by increasing the mismatch, suggesting a possible correlation, for example arising from the strain-induced modulation of certain bond distortions. The same clear correlation is not observed for the 12 u.c. samples. For samples above conduction threshold, however, we expect a more complex behavior. Indeed, in this case, it is plausible to assume that two different sources of interfacial polarity contribute to the SHG process in the investigated perovskite oxide interfaces: structural proximity effects, which may be strongly affected by strain, and space-charge effects arising from charge injection, which are presumably insensitive or weakly sensitive to strain. Hence, when the latter effect dominates, as it occurs for 12 u.c., the correlation of the SHG intensity to the strain might be lost.

VI. CONCLUSIONS

We have performed a detailed investigation of polar/nonpolar STO-based heterostructures by means of SHG spectroscopy. SHG spectra have been recorded up to a two-photon energy of 4.2 eV while varying different parameters: film thickness, temperature, and overlayer material. For the latter, we have used LAO, NGO, and LGO, all with a perovskite structure. Within the range of the varied parameters, we find that the $4mm$ symmetry of these interfaces is generally preserved, although with few noticeable deviations. This conclusion can be drawn because all the sp spectra show an almost full suppression of the peak at 3.6 eV present in the ds spectra, thus confirming what is expected from the selection rules controlled by the $4mm$ symmetry. Besides, we have found an overall enhancement of second harmonic signal at low temperature, indicating an increase of the interfacial polarity with decreasing temperature. This confirms the picture about the origin of second harmonic signal as a consequence of the spatial translation of Ti ions, more prone to move at lower temperatures because of the paraelectric nature of STO.

As anticipated, slight deviations from the general picture dictated by the symmetry selection rules have been observed. In particular, the suppression of the 3.6-eV peak in the

sp spectra is not always complete. This demonstrates that symmetry is partly lifted due to proximity effects, as, for example, distortions of the TiO_6 octahedra possibly induced by LAO in STO at the interface or bond buckling. Another noticeable finding is the correlation between the SHG signal and the in-plane lattice mismatch of LAO/STO, NGO/STO, and LGO/STO interfaces, observed when the number of deposited layers is too low for inducing conduction. In this case, SHG spectroscopy proves to be able to detect substrate distortions that are probably induced or at least modulated by strain. All these additional results show the potential of the SHG spectroscopy in capturing subtle structural details of these interfaces.

ACKNOWLEDGMENT

We acknowledge funding from the European Union (Programme FP7/2007-2013, Grant Agreement No. 264098-MAMA; FP7-PEOPLE-2012-CIG, Grant Agreement No. PCIG12-GA-2012-326499-FOXIDUET), by the Ministero dell'Istruzione, dell'Università e della Ricerca (Grant No. PRIN 2010-11-OXIDE), by the Deutsche Forschungsgemeinschaft (SFB 608 and TRR 80).

*domenico.paparo@spin.cnr.it

¹R. Ramesh and D. G. Schlom, *MRS Bull.* **33**, 1006 (2008).

²A. Ohtomo and H. Hwang, *Nature (London)* **427**, 423 (2004).

³N. Nakagawa, H. Y. Hwang, and D. A. Muller, *Nat. Mater.* **5**, 204 (2006).

⁴S. Thiel, G. Hammerl, A. Schmehl, C. Schneider, and J. Mannhart, *Science* **313**, 1942 (2006).

⁵A. Brinkman, M. Huijben, M. V. Zalk, J. Huijben, U. Zeitler, J. C. Maan, W. G. V. der Wiel, G. Rijnders, D. H. A. Blank, and H. Hilgenkamp, *Nat. Mater.* **6**, 493 (2007).

⁶N. Reyren, S. Thiel, A. Caviglia, L. Fitting Kourkoutis, G. Hammerl, C. Richter, C. Schneider, T. Kopp, A.-S. Rüetschi, D. Jaccard, M. Gabay, D. Muller, J.-M. Triscone, and J. Mannhart, *Science* **317**, 1196 (2007).

⁷C. Cen, S. Thiel, G. Hammerl, C. Schneider, K. Andersen, C. Hellberg, J. Mannhart, and J. Levy, *Nat. Mater.* **7**, 298 (2008).

⁸M. Basletic, J.-L. Maurice, C. Carrétéro, G. Herranz, O. Copie, M. Bibes, E. Jacquet, K. Bouzouane, S. Fusil, and A. Barthélémy, *Nat. Mater.* **7**, 621 (2008).

⁹K. Yoshimatsu, R. Yasuhara, H. Kumigashira, and M. Oshima, *Phys. Rev. Lett.* **101**, 026802 (2008).

¹⁰A. Caviglia, S. Gariglio, N. Reyren, D. Jaccard, T. Schneider, M. Gabay, S. Thiel, G. Hammerl, J. Mannhart, and J.-M. Triscone, *Nature (London)* **456**, 624 (2008).

¹¹M. Huijben, A. Brinkman, G. Koster, G. Rijnders, H. Hilgenkamp, and D. H. A. Blank, *Adv. Mater.* **21**, 1665 (2009).

¹²P. Zubko, S. Gariglio, M. Gabay, P. Ghosez, and J.-M. Triscone, *Annu. Rev. Condens. Matter Phys.* **2**, 141 (2011).

¹³M. Huijben, G. Rijnders, D. H. A. Blank, S. Bals, S. V. Aert, J. Verbeeck, G. V. Tendeloo, A. Brinkman, and H. Hilgenkamp, *Nat. Mater.* **5**, 556 (2006).

¹⁴A. Tsukazaki, A. Ohtomo, T. Kita, Y. Ohno, H. Ohno, and M. Kawasaki, *Science* **315**, 1388 (2007).

¹⁵T. Higuchi, Y. Hotta, T. Susaki, A. Fujimori, and H. Y. Hwang, *Phys. Rev. B* **79**, 075415 (2009).

¹⁶A. Ohtomo, D. A. Muller, J. L. Grazul, and H. Y. Hwang, *Nature (London)* **419**, 378 (2002).

¹⁷Y. Hotta, T. Susaki, and H. Y. Hwang, *Phys. Rev. Lett.* **99**, 236805 (2007).

¹⁸C. Cantoni, J. Gazquez, F. M. Granozio, M. P. Oxley, M. Varela, A. R. Lupini, S. J. Pennycook, C. Aruta, U. Scotti di Uccio, P. Perna, and D. Maccariello, *Adv. Mater.* **24**, 3952 (2012).

¹⁹H. Hwang, *Science* **313**, 1895 (2006).

²⁰C. Cen, S. Thiel, J. Mannhart, and J. Levy, *Science* **323**, 1026 (2009).

²¹G. Herranz, M. Basletic, M. Bibes, C. Carretero, E. Tafra, E. Jacquet, K. Bouzouane, C. Deranlot, A. Hamzic, J. M. Broto, A. Barthelemy, and A. Fert, *Phys. Rev. Lett.* **98**, 216803 (2007).

²²W. Siemons, G. Koster, H. Yamamoto, W. A. Harrison, G. Lucovsky, T. H. Geballe, D. H. A. Blank, and M. R. Beasley, *Phys. Rev. Lett.* **98**, 196802 (2007).

²³A. Kalabukhov, R. Gunnarsson, J. Borjesson, E. Olsson, T. Claeson, and D. Winkler, *Phys. Rev. B* **75**, 121404 (2007).

²⁴S. A. Pauli and P. R. Willmott, *J. Phys.: Condens. Matter* **20**, 264012 (2008).

²⁵A. S. Kalabukhov, Y. A. Boikov, I. T. Serenkov, V. I. Sakharov, V. N. Popok, R. Gunnarsson, J. Borjesson, N. Ljustina, E. Olsson, D. Winkler, and T. Claeson, *Phys. Rev. Lett.* **103**, 146101 (2009).

²⁶Y. Chen, N. Pryds, J. E. Kleibeuker, G. Koster, J. Sun, E. Stamate, B. Shen, G. Rijnders, and S. Linderth, *Nano Lett.* **11**, 3774 (2011).

²⁷M. L. Reinle-Schmitt, C. Cancellieri, D. Li, D. Fontaine, M. Medarde, E. Pomjakushina, C. W. Schneider, S. Gariglio, P. Ghosez, J. M. Triscone, and P. R. Willmott, *Nat. Commun.* **3**, 932 (2012).

- ²⁸C. Cancellieri, D. Fontaine, S. Gariglio, N. Reyren, A. D. Caviglia, A. Fete, S. J. Leake, S. A. Pauli, P. R. Willmott, M. Stengel, P. Ghosez, and J. M. Triscone, *Phys. Rev. Lett.* **107**, 056102 (2011).
- ²⁹S. A. Pauli, S. J. Leake, B. Delley, M. Bjorck, C. W. Schneider, C. M. Schlepütz, D. Martoccia, S. Paetel, J. Mannhart, and P. R. Willmott, *Phys. Rev. Lett.* **106**, 036101 (2011).
- ³⁰Z. Q. Liu, C. J. Li, W. M. Lü, X. H. Huang, Z. Huang, S. W. Zeng, X. P. Qiu, L. S. Huang, A. Annadi, J. S. Chen, J. M. D. Coey, T. Venkatesan, and Ariando, *Phys. Rev. X* **3**, 021010 (2013).
- ³¹M. Breitschaft, V. Tinkl, N. Pavlenko, S. Paetel, C. Richter, J. R. Kirtley, Y. C. Liao, G. Hammerl, V. Eyert, T. Kopp, and J. Mannhart, *Phys. Rev. B* **81**, 153414 (2010).
- ³²B. C. Huang, Y. P. Chiu, P. C. Huang, W. C. Wang, V. T. Tra, J. C. Yang, Q. He, J. Y. Lin, C. S. Chang, and Y. H. Chu, *Phys. Rev. Lett.* **109**, 246807 (2012).
- ³³G. Drera, G. Salvinelli, A. Brinkman, M. Huijben, G. Koster, H. Hilgenkamp, G. Rijnders, D. Visentin, and L. Sangaletti, *Phys. Rev. B* **87**, 075435 (2013).
- ³⁴G. Berner, M. Sing, H. Fujiwara, A. Yasui, Y. Saitoh, A. Yamasaki, Y. Nishitani, A. Sekiyama, N. Pavlenko, T. Kopp, C. Richter, J. Mannhart, S. Suga, and R. Claessen, *Phys. Rev. Lett.* **110**, 247601 (2013).
- ³⁵M. Salluzzo, J. C. Cezar, N. B. Brookes, V. Bisogni, G. M. De Luca, C. Richter, S. Thiel, J. Mannhart, M. Huijben, A. Brinkman, G. Rijnders, and G. Ghiringhelli, *Phys. Rev. Lett.* **102**, 166804 (2009).
- ³⁶M. Sing, G. Berner, K. Goss, A. Müller, A. Ruff, A. Wetscherek, S. Thiel, J. Mannhart, S. A. Pauli, C. W. Schneider, P. R. Willmott, M. Gorgoi, F. Schäfers, and R. Claessen, *Phys. Rev. Lett.* **102**, 176805 (2009).
- ³⁷C. Cancellieri, M. L. Reinle-Schmitt, M. Kobayashi, V. N. Strocov, T. Schmitt, P. R. Willmott, S. Gariglio, and J. M. Triscone, *Phys. Rev. Lett.* **110**, 137601 (2013).
- ³⁸M. Salluzzo, S. Gariglio, X. Torrelles, Z. Ristic, R. Di Capua, J. Drnec, M. M. Sala, G. Ghiringhelli, R. Felici, and N. B. Brookes, *Adv. Mater.* **25**, 2333 (2013).
- ³⁹S. S. A. Seo, M. J. Han, G. W. J. Hassink, W. S. Choi, S. J. Moon, J. S. Kim, T. Susaki, Y. S. Lee, J. Yu, C. Bernhard, H. Y. Hwang, G. Rijnders, D. H. A. Blank, B. Keimer, and T. W. Noh, *Phys. Rev. Lett.* **104**, 036401 (2010).
- ⁴⁰Y. R. Shen, *Appl. Phys. A* **59**, 541 (1994).
- ⁴¹M. Bonn, A. W. Kleyn, and G. J. Kroes, *Surf. Sci.* **500**, 475 (2002).
- ⁴²A. Kirilyuk, *J. Phys. D* **35**, R189 (2002).
- ⁴³A. Savoia, D. Paparo, P. Perna, Z. Ristic, M. Salluzzo, F. Miletto Granozio, U. Scotti di Uccio, C. Richter, S. Thiel, J. Mannhart, and L. Marrucci, *Phys. Rev. B* **80**, 075110 (2009).
- ⁴⁴N. Ogawa, K. Miyano, M. Hosoda, T. Higuchi, C. Bell, Y. Hikita, and H. Y. Hwang, *Phys. Rev. B* **80**, 081106 (2009).
- ⁴⁵A. Rubano, M. Fiebig, D. Paparo, A. Marino, D. Mac-carriello, U. Scotti di Uccio, F. Miletto Granozio, L. Marrucci, C. Richter, S. Paetel, and J. Mannhart, *Phys. Rev. B* **83**, 155405 (2011).
- ⁴⁶T. Günter, A. Rubano, D. Paparo, M. Lilienblum, L. Marrucci, F. Miletto Granozio, U. Scotti di Uccio, R. Jany, C. Richter, J. Mannhart, and M. Fiebig, *Phys. Rev. B* **86**, 235418 (2012).
- ⁴⁷A. Rubano, T. Günter, T. Fink, D. Paparo, L. Marrucci, C. Cancellieri, S. Gariglio, J.-M. Triscone, and M. Fiebig, *Phys. Rev. B* **88**, 035405 (2013).
- ⁴⁸D. Paparo, A. Rubano, and L. Marrucci, *J. Opt. Soc. Am. B* **30**, 2452 (2013).
- ⁴⁹A. H. Kahn and A. J. Leyendecker, *Phys. Rev.* **135**, A1321 (1964).
- ⁵⁰L. F. Mattheiss, *Phys. Rev. B* **6**, 4718 (1972).
- ⁵¹K. van Benthem, C. Elsässer, and R. H. French, *J. Appl. Phys.* **90**, 6156 (2001).
- ⁵²W. Luo, W. Duan, S. G. Louie, and M. L. Cohen, *Phys. Rev. B* **70**, 214109 (2004).
- ⁵³P. N. Butcher and D. Cotter, *The Elements of Nonlinear Optics* (Cambridge University Press, Cambridge, UK, 1990).
- ⁵⁴D. C. Harris and M. D. Bertolucci, *Symmetry and Spectroscopy: An Introduction to Vibrational and Electronic Spectroscopy* (Dover, New York 1989).
- ⁵⁵A. F. Santander-Syro, O. Copie, T. Kondo, F. Fortuna, S. Pailhes, R. Weht, X. G. Qiu, F. Bertran, A. Nicolaou, A. Taleb-Ibrahimi, P. Le Fevre, G. Herranz, M. Bibes, N. Reyren, Y. Apertet, P. Lecoeur, A. Barthelemy, and M. J. Rozenberg, *Nature (London)* **469**, 189 (2011).
- ⁵⁶Z. S. Popović, S. Satpathy, and R. M. Martin, *Phys. Rev. Lett.* **101**, 256801 (2008).
- ⁵⁷P. Delugas, A. Filippetti, V. Fiorentini, D. I. Bilc, D. Fontaine, and P. Ghosez, *Phys. Rev. Lett.* **106**, 166807 (2011).
- ⁵⁸M. Cardona, *Phys. Rev.* **140**, A651 (1965).
- ⁵⁹V. Trepakov, A. Dejneka, P. Markovin, A. Lynnyk, and L. Jastrabik, *New J. Phys.* **11**, 083024 (2009).
- ⁶⁰K. A. Müller and H. Burkard, *Phys. Rev. B* **19**, 3593 (1979).
- ⁶¹A. Savoia, M. Siano, D. Paparo, and L. Marrucci, *J. Opt. Soc. Am. B* **28**, 679 (2011).
- ⁶²C. L. Jia, S. B. Mi, M. Faley, U. Poppe, J. Schubert, and K. Urban, *Phys. Rev. B* **79**, 081405 (2009).
- ⁶³We define the in-plane lattice mismatch between the STO substrate and the bulk material to be deposited as $m = (a_{\text{STO}} - a_{\text{bulk}})/a_{\text{STO}}$, where a_{STO} is the cubic lattice parameter of STO, being equal to 0.39 nm, while a_{bulk} is the pseudocubic lattice parameter of LGO, NGO, and LAO, being 0.389, 0.386, and 0.378 nm, respectively. Therefore, m is approximately equal to 0.38%, 1.15%, and 3.2% for LGO/STO, NGO/STO, and LAO/STO, respectively.